A novel method for deriving the diffraction transfer matrix and its application to multi-body interactions in water waves

A novel method for deriving the diffraction transfer matrix and its application to multi-body interactions in water waves

J. Cameron McNatt*, Vengatesan Venugopal, David Forehand

Institute for Energy Systems, School of Engineering, The University of Edinburgh Edinburgh, EH9 3JL, United Kingdom

Abstract

A matrix method was developed by Kagemoto and Yue (1986) to compute interactions between multiple three-dimensional bodies subjected to linear water waves. The approach leads to a significant reduction in computational time versus the direct method, in which the boundary value problem is solved for all bodies simultaneously. An essential component of the theory is the so-called diffraction transfer matrix, a linear operator defined for each unique geometry. However, the diffraction transfer matrix is not a standard product of a linear wave computation, for one, because it is based around an unusual representation of incident waves, that is, as partial cylindrical waves. In this paper, a new method is presented to compute the diffraction transfer matrix from plane incident waves, which enables one to derive it from standard wave-body software or experiments. Additionally, a new linear operator - the force transfer matrix, is presented, which can also be determined by usual means. Herein, the interaction theory calculation is verified against direct method results from the linear wave-body software, WAMIT, and then applied to compute absorbed power and wave field effects on a medium-sized array in spectral seas and on a large farm of 101 wave energy converters in regular waves.

Keywords: multiple scattering, wave energy converter, wave farm, wave field, diffraction transfer matrix

*Corresponding author

Email address: c.mcnatt@ed.ac.uk (J. Cameron McNatt)

1. Introduction

The computation of water wave interaction effects amongst fixed or floating bodies is important to the analysis of a variety of offshore and coastal problems. For example, research was conducted in the 1990s on the design of very large floating structures, supported by on the order of 100 floating legs, whose purposes would be to expand usable space into the sea, such as for floating airports (Kagemoto and Yue, 1993; Murai et al., 1999; Kashiwagi, 2000). In the arctic and antarctic regions, interactions between large fields of icebergs in the marginal ice zone are important to environmental dynamics (Peter et al., 2006). In the emerging field of offshore renewable energy, to generate cost-effective electricity, devices, such as offshore wind turbines and wave energy converters (WECs), must be deployed in arrays, known as farms, where wave interactions will have significant effects on wave loads, dynamics, and performance.

The initial approach to the analysis of floating body arrays is to compute first-order forces and motions with linear wave theory. Kagemoto and Yue (1986) developed a very powerful theory, often called an interaction theory, for the computation of the linear wave forces on a body due to the presence of other bodies. The interaction theory is exact within limits of linear wave theory, accounts for both progressive and evanescent waves, and has only a minimal restriction with respect to the bodies' positions. The essence of the theory is that hydrodynamic properties only need to be computed for each unique geometry and the interaction effects between multiple geometries are computed with linear algebra based on the knowledge that waves scattered and radiated by one body are the incident waves on another. For an array of devices of the same geometry, the method provides significant computational savings over the direct method of computing linear wave effects on an array. In the direct method, the linear-wave boundary value problem is solved using the surface of all bodies simultaneously, and is typically performed computationally with a boundary element method (BEM) solver. In contrast, the Kagemoto and Yue (1986) interaction theory uses a linear operator called a diffraction transfer matrix that represents the scattering properties of body and is found by solving the BVP for the body in isolation. The diffraction transfer matrix transform vectors of incident, cylindrical, partial-wave coefficients into a vectors of outgoing, partial-wave coefficients representing waves scattered by the body.

Analogous theories for multi-body wave interactions can also be found in

the fields of electromagnetism and acoustics, many of which have preceded and guided hydrodynamic ones. In these theories, the diffraction transfer matrix is referred to as a T-matrix (for transition matrix). An extensive treatment of multi-body wave scattering in a variety of fields can be found in Martin (2006).

For an isolated, bottom-mounted, circular cylinder, the coefficients of the scattered wave can be determined in a straightforward manner from the body-boundary condition (MacCamy and Fuchs, 1954). Garrett (1971) devised an analytical technique to find the scattered-wave coefficients for a floating truncated cylinder. Recently, Wypych et al. (2012) discussed the circular-cylindrical solutions of radiated waves from a point-absorber type WEC moving in heave and surge. In that paper, they considered wave power absorption and showed experimentally that the solutions are accurate within the limits of linear wave theory. McNatt et al. (2013) demonstrated that arbitrary geometries can be represented by cylindrical waves and presented a new method to compute cylindrical wave coefficients for any geometry with values measured in a numerical or experimental linear wave field.

Considering the array problem, Yilmaz (1998) applied the Kagemoto and Yue (1986) method to multiple truncated floating cylinders using the analytical solution of Garrett (1971) to a single cylinder to compute the diffraction transfer matrix and hydrodynamic forces. Following Yilmaz, Child and Venugopal (2010) considered truncated floating cylinders as an array of WECs and due to the speed of the computation were able to use a genetic algorithm to optimize the WEC array layout. For complex geometries where no analytical solution is readily available, numerical methods are required to determine the diffraction transfer matrix. Kagemoto and Yue (1986) used a hybrid-element method (HEM) to compute it for an axisymmetric body. For a general shape, Goo and Yoshida (1990) and later Chakrabarti (2000) used a BEM based on Fourier-series cylindrical Green functions developed by Fenton (1978). A significant difficulty with both of these methods is that to implement them a custom HEM or BEM code needs to be developed. To the authors' knowledge, no commercial or publicly available hydrodynamic software produces the coefficients required for the hydrodynamic interaction theory. Furthermore, it would not be straightforward to modify standard BEM software, which uses Cartesian Green functions, to produce the diffraction transfer matrix, as this would necessitate changing both the incident wave as well as the Green functions. This severely undermines the simplicity of Kagemoto and Yue (1986)'s method and has relegated this powerful

method to infrequent use in favor of direct computation with commercial BEM software.

Following the work of McNatt et al. (2013), herein, a method is presented for computing the diffraction transfer matrix by probing a body with plane incident waves. The method is straight-forward and can be performed with results from most standard software or experiments as long as linearity is assumed or given. A novel operator called the force transfer matrix is introduced. The force transfer matrix transforms a vector of incident partial cylindrical wave coefficients into forces on the body. It is used in both the diffraction and radiation problems, and is computed in a manner similar to that of the diffraction transfer matrix. With the inclusion of the force transfer matrix, the interaction problem becomes purely algebraic and programming it is relatively uncomplicated.

A deficiency of the method presented here is that only propagating wave modes are included. This is unavoidable because only propagating incident waves are practical to use to compute the diffraction transfer and force transfer matrices. The absence of evanescent wave modes results in differences as compared to a full linear wave theory computation when bodies are spaced very close together. However, it is shown for the geometries considered in this paper that this error is very small and is negligible for most inter-body spacings of practical interest. Although one may view this as a wide-spacing approximation, it is different from another well-known, wide-spacing approach - the plane-wave approximation (Simon, 1982). In the method herein, propagating radiated and scattered waves are modeled exactly as curved waves to the limit of their truncation values, while in the plane-wave approximation, these waves are approximated as plane-waves incident on other bodies.

In the following sections, the methodology for deriving the diffraction transfer and force transfer matrices and the results from their applications to interaction theory are presented. First, the cylindrical wave solution to the linear-wave boundary-value problem and its notation are shown. Next, Kagemoto and Yue (1986)'s interaction theory is reviewed, into which the novel force transfer matrix is introduced for the computation of excitation forces and the added mass and damping matrices. Then, new techniques are presented for deriving the diffraction transfer and force transfer matrices from incident plane waves. Following the methodology, a summary section is presented to further clarify the computational procedures. Results are shown for a cylinder and an attenuator-type WEC and verified with comparison to direct computation using the BEM software, WAMIT (WAMIT User Man-

ual, Version 7.0, 2012). Finally, the method is used to compute the power absorption and wave field of a medium-sized array of WECs in spectral seas and of a very large wave farm of 101 WECs in regular waves - computations that are not practical with direct methods given current computational resources.

2. Interaction problem

The problem considered here is the linear wave-body boundary value problem (BVP), with the usual assumptions and boundary conditions (see Newman, 1977, Chap. 6), including an incompressible, irrotational fluid, a flat bottom, small body motions, and a linearized free-surface boundary condition. Fluid motions are sinusoidal with time, so that the velocity potential, Φ, can be separated into a spatially dependent quantity, ϕ, and a time dependent quantity, $\Phi = \mathrm{Re}\left\{\phi\left(\boldsymbol{x}\right) e^{\mathrm{i}\omega t}\right\}$, where $\boldsymbol{x}$ is the spatial coordinates, t is time, $\mathrm{i} = \sqrt{-1}$, and ω is the radial frequency. For an array of floating bodies in proximity to one another, the velocity potential is the superposition of an incident wave potential, ϕ^I, scattered wave potentials due to all bodies when held fixed, ϕ^S, and the radiation potentials, $\phi^R_{q_i}$ due to each body i, moving in each of its degrees-of-freedom, q_i,

$$\phi = \phi^I + \phi^S + \sum_{i=1}^{N} \sum_{q_i=1}^{Q_i} \zeta_{q_i} \phi^R_{q_i} \tag{1}$$

where ζ_{q_i} is the amplitude of the generalized motion of mode q_i and Q_i is the total number of degrees-of-freedom of body i. N is the total number of bodies and $Q = \sum_{i=1}^{N} Q_i$ is the total number of degrees-of-freedom of the array.

The BVP can be solved for the interaction between bodies in the array under the assumption that hydrodynamic quantities for each body are known. This is called an interaction problem. The necessary hydrodynamic quantities are the added mass and damping, the diffraction transfer matrix, and the force transfer matrix. The added mass and damping are familiar quantities and their derivation is well known. The diffraction transfer matrix is essential to this interaction theory and although not as widely employed, it is not new to literature. The force transfer matrix is a new quantity introduced herein. The derivations of the diffraction transfer matrix and the

force transfer matrix are given in Section 3, and their meanings are discussed throughout this paper.

The interaction problem described in this section follows that of Kagemoto and Yue (1986) with a few differences in notation. Lower-case $\boldsymbol{a}$ is used for partial wave amplitudes, where superscripts distinguish the type of wave instead of Kagemoto and Yue (1986) use of capital $\boldsymbol{A}$ for the scattered wave amplitudes and lower-case $\boldsymbol{a}$ for the planar incident wave amplitudes. The transformation matrix has the same notation, T_{ij}, but the opposite meaning - $\boldsymbol{\Psi}_j^S = \mathsf{T}_{ij}\boldsymbol{\Psi}_i^I$ rather than Kagemoto and Yue (1986) $\boldsymbol{\Psi}_i^S = \mathsf{T}_{ij}\boldsymbol{\Psi}_j^I$, because the usage herein results in a more logical matrix equation for the complete system, as shall be seen at the end of this section. And so, instead of the interaction being solved about a body j, as in Kagemoto and Yue (1986), the problem is solved about body i. D_i rather than $\boldsymbol{B}_j$, is used to denote the diffraction transfer matrix. And finally, only propagating wave modes are considered.

2.1. Cylindrical wave solutions about isolated bodies

A solution to be BVP in the absence of bodies is a long-crested plane wave, which can be written in the cylindrical coordinates about body i, $\{r_i, \theta_i, z\}$, as the product of infinitely long vectors of coefficients and basis functions:

$$\phi_i^P(\beta) = \mathrm{i}\frac{\mathrm{g}}{\omega}\left(\boldsymbol{a}_i^P\right)^{\mathsf{T}}\boldsymbol{\Psi}_i^I \tag{2}$$

where g is the gravitational constant, and T indicates the vector transpose. $\boldsymbol{a}_i^P$ is a vector of coefficients (the superscript P indicates a plane wave, and the subscript i indicates the i^{th} body) whose m^{th} coefficient is

$$\left(\boldsymbol{a}_i^P\right)_m = Ae^{-\mathrm{i}k_0(X_i\cos\beta + Y_i\sin\beta)}e^{-\mathrm{i}m\left(\beta+\frac{\pi}{2}\right)} \tag{3}$$

where A is a the complex wave amplitude; k_0 is the propagating wave number; β is the wave heading (angle relative to the positive body x_i-axis, where $x_i = r_i\cos\theta_i$, $y_i = r_i\sin\theta_i$); $\{X_i, Y_i\}$ is the position of body i in a global coordinate system; and the body axis x_i is parallel to the global X axis. $\boldsymbol{\Psi}_i^I$ is a vector of incident basis functions (the superscript I indicates an incident wave) whose m^{th} value is

$$\left(\boldsymbol{\Psi}_i^I\right)_m = \frac{\cosh k_0(h+z)}{\cosh k_0 h}J_m(k_0 r_i)\,e^{\mathrm{i}m\theta_i} \tag{4}$$

where h is the water depth, and J_m is the m^{th} order Bessel function of the first kind.

In an analogous manner, considering for now only the propagating wave modes, the velocity potential of the waves scattered (superscript S) or radiated (superscript R) by a floating body i can be written as product of complex coefficients and scattered basis functions

$$\phi_i^{S,R} = \mathrm{i}\frac{\mathrm{g}}{\omega}\left(\boldsymbol{a}_i^{S,R}\right)^{\mathsf{T}}\boldsymbol{\Psi}_i^S \tag{5}$$

where $\boldsymbol{a}_i^{S,R}$ is a vector of the coefficients that depend on the geometry and for radiated waves the mode of motion, of body i. $\boldsymbol{\Psi}_i^S$ is a vector of scattered basis functions (which also apply to radiated waves)

$$\left(\boldsymbol{\Psi}_i^S\right)_m = \frac{\cosh k_0\left(h+z\right)}{\cosh k_0 h}H_m^{(2)}\left(k_0 r_i\right)e^{\mathrm{i}m\theta_i} \tag{6}$$

where $H_m^{(2)}$ is the m^{th} order Hankel function of the second kind. In some cases, the Bessel of Hankel functions in the basis functions are normalized (e.g. (Child and Venugopal, 2010)), however, here they are not.

In general the coefficient and basis function vectors are infinitely long, and their scalar product is an infinite summation centered about $m = 0$. In practice, this is truncated with a value M, so that the summation goes from $m = -M$ to M.

2.2. Solution to the interaction problem

For an array of N fixed bodies, the incident waves to a given body i are the sum of the ambient incident waves, $\phi_i^A = \mathrm{i}\frac{\mathrm{g}}{\omega}\left(\boldsymbol{a}_i^A\right)^{\mathsf{T}}\boldsymbol{\Psi}_i^I$, and waves scattered by all other bodies, $\phi_j^S = \mathrm{i}\frac{\mathrm{g}}{\omega}\left(\boldsymbol{a}_j^S\right)^{\mathsf{T}}\boldsymbol{\Psi}_j^S$.

$$\phi_i^I = \mathrm{i}\frac{\mathrm{g}}{\omega}\left(\left(\boldsymbol{a}_i^A\right)^{\mathsf{T}}\boldsymbol{\Psi}_i^I + \sum_{\substack{j=1\\ j\neq i}}^{N}\left(\boldsymbol{a}_j^S\right)^{\mathsf{T}}\boldsymbol{\Psi}_j^S\right) \tag{7}$$

Here, the terminology "incident wave" means any wave component traveling towards a body. The ambient incident waves are the waves that drive the hydrodynamic interaction - without them, there would be no scattered

waves. However, they are not necessarily plane incident waves; in the radiation problem, they are the radiated waves. The scattered waves of each body are the result of scattering of the ambient incident wave and scattering of incident waves that are the scattered waves of other bodies.

The relationship between an m^{th} order Hankel function of the second kind in body coordinate system i and an n^{th} order Bessel function of the first kind in body coordinate system j is given by Graf's addition theorem (Abrmowitz and Stegun, 1964):

$$H_m^{(2)}\left(k_0 r_j\right) e^{\mathrm{i}m\theta_j} = \sum_{n=-\infty}^{\infty} H_{m-n}^{(2)}\left(k_0 L_{ij}\right) e^{\mathrm{i}(m-n)\alpha_{ij}} J_n\left(k_0 r_i\right) e^{\mathrm{i}n\theta_i} \tag{8}$$

where $L_{ij} = \sqrt{\left(X_i - X_j\right)^2 + \left(Y_i - Y_j\right)^2}$ and $\alpha_{ij} = \arctan\left(\frac{Y_i - Y_j}{X_i - X_j}\right)$, and are the distance and angle respectively of body i to body j. (Again, j and i are switched as compared to Kagemoto and Yue (1986)). Define a transformation matrix, $\mathbf{T}_{ij}$, that transforms incident basis functions in the coordinates of body i into scattered basis functions in the coordinates of body j, $\mathbf{\Psi}_j^S = \mathbf{T}_{ij}\mathbf{\Psi}_i^I$. The mn^{th} element of the transformation matrix $\mathbf{T}_{ij}$ is

$$\left(\mathbf{T}_{ij}\right)_{mn} = H_{m-n}^{(2)}\left(k_0 L_{ij}\right) e^{\mathrm{i}(m-n)\alpha_{ij}} \tag{9}$$

Applying equation 9 to equation 7, the waves incident to body i in terms of incident basis functions of i are

$$\phi_i^I = \mathrm{i}\frac{\mathrm{g}}{\omega}\left(\left(\boldsymbol{a}_i^A\right)^{\mathsf{T}} + \sum_{\substack{j=1 \\ j\neq i}}^{N}\left(\boldsymbol{a}_j^S\right)^{\mathsf{T}}\mathbf{T}_{ij}\right)\mathbf{\Psi}_i^I \tag{10}$$

Equation 10 is of the form, $\phi_i^I = \mathrm{i}\frac{\mathrm{g}}{\omega}\left(\boldsymbol{a}_i^I\right)^{\mathsf{T}}\mathbf{\Psi}_i^I$, where the incident wave coefficients, $\boldsymbol{a}_i^I$, are the sum of the ambient incident waves and the transformed scattered waves from all other bodies.

Now consider the diffraction transfer matrix of body i. The diffraction transfer matrix is a linear operator that transforms incident wave amplitudes to body i into the scattered wave amplitudes of body i, $\boldsymbol{a}_i^S = \mathbf{D}_i\boldsymbol{a}_i^I$. With the use of the diffraction transfer matrix, equation 10 becomes

$$\boldsymbol{a}_i^S = \mathbf{D}_i \left(\boldsymbol{a}_i^A + \sum_{\substack{j=1 \\ j \neq i}}^{N} \mathbf{T}_{ij}^{\mathsf{T}} \boldsymbol{a}_j^S \right) \tag{11}$$

If the ambient incident wave amplitudes and the diffraction transfer matrices are known, then the scattered wave amplitudes can be found by solving equation 11 as a system of linear equations in the form

$$\begin{aligned} \begin{bmatrix} \boldsymbol{a}_1^S \\ \boldsymbol{a}_2^S \\ \vdots \\ \boldsymbol{a}_N^S \end{bmatrix} = & \begin{bmatrix} \mathbf{D}_1 & \mathbf{0} & \cdots & \mathbf{0} \\ \mathbf{0} & \mathbf{D}_2 & & \vdots \\ \vdots & & \ddots & \mathbf{0} \\ \mathbf{0} & \cdots & \mathbf{0} & \mathbf{D}_N \end{bmatrix} \\ & \times \left(\begin{bmatrix} \boldsymbol{a}_1^A \\ \boldsymbol{a}_2^A \\ \vdots \\ \boldsymbol{a}_N^A \end{bmatrix} + \begin{bmatrix} \mathbf{0} & \mathbf{T}_{12}^{\mathsf{T}} & \cdots & \mathbf{T}_{1N}^{\mathsf{T}} \\ \mathbf{T}_{21}^{\mathsf{T}} & \mathbf{0} & & \vdots \\ \vdots & & \ddots & \mathbf{T}_{(N-1)N}^{\mathsf{T}} \\ \mathbf{T}_{N1}^{\mathsf{T}} & \cdots & \mathbf{T}_{N(N-1)}^{\mathsf{T}} & \mathbf{0} \end{bmatrix} \begin{bmatrix} \boldsymbol{a}_1^S \\ \boldsymbol{a}_2^S \\ \vdots \\ \boldsymbol{a}_N^S \end{bmatrix} \right) \end{aligned} \tag{12}$$

Here the advantage of using the given definition of $\mathbf{T}_{ij}$ becomes apparent - $\mathbf{T}_{ij}$ means the i^{th} row j^{th} column transformation matrix of the super transformation matrix.

2.3. Forces due to the interaction problem

The incident waves on each body resulting from the interaction theory are a summation of partial cylindrical waves of various amplitudes. Because Kagemoto and Yue (1986), and subsequent authors who employed their method, had software designed to handle cylindrical incident waves, they could compute excitation force by solving the BVP for incident cylindrical partial waves and then directly integrating the dynamic pressure. Unfortunately, standard, linear-wave software only solves for forces due to incident plane waves.

To overcome this short-coming, and in keeping with the simplicity of the diffraction transfer matrix, another linear operator, which can be derived from plane incident waves, is introduced to compute the forces - the force

transfer matrix. The force transfer matrix, $\mathbf{G}_i$, transforms incident partial wave amplitudes on body i into linear excitation forces on body i in each degree of freedom, $\boldsymbol{f}_i = \mathbf{G}_i \boldsymbol{a}_i^I$. The derivation of the force transfer matrix is given in section 3.3.

2.3.1. Excitation forces due to planar incident waves

For the excitation forces on all bodies held fixed due to an incident plane wave at a direction, β, the ambient incident wave amplitudes are given by $\boldsymbol{a}_i^A = \boldsymbol{a}_i^P(\beta)$ (equation 3). The scattered wave problem is solved as described in subsection 2.2. The incident waves to body i are the quantities in the brackets in equation 11, and the excitation force on body i is

$$\boldsymbol{f}_i^E(\beta) = \mathbf{G}_i \left(\boldsymbol{a}_i^P(\beta) + \sum_{\substack{j=1 \\ j \neq i}}^{N} \mathbf{T}_{ij}^{\mathsf{T}} \boldsymbol{a}_j^S \right) \tag{13}$$

2.3.2. Added mass and damping matrices

The added mass, $\mathbf{A}$, and damping, $\mathbf{B}$, matrices for the complete system are found by solving an interaction problem for each degree of freedom of the entire array. For motion of the q_j^{th} mode, the ambient incident wave amplitudes to body i are the transformed radiated wave amplitudes, $\mathbf{T}_{ij}^{\mathsf{T}} \boldsymbol{a}_{q_j}^R$, where $\boldsymbol{a}_{q_j}^R$ are the radiated wave amplitudes of body j moving in mode q_j. On body j the ambient incident waves are are zero.

$$\boldsymbol{a}_{i,q_j}^A = \begin{cases} \mathbf{T}_{ij}^{\mathsf{T}} \boldsymbol{a}_{q_j}^R & i \neq j \\ \mathbf{0} & i = j \end{cases} \tag{14}$$

For all bodies beside the body undergoing motion, the radiation force is due solely to incident waves from other bodies. For the body undergoing the motion, the total radiation force must include the radiation forces of the body on itself, that is, its own added mass and damping matrices. The radiation force on body i due to motion in mode q_j is

$$\left(\mathbf{F}_i^R\right)_{\bullet q_j} = \begin{cases} \mathbf{G}_i \boldsymbol{a}_i^I & i \neq j \\ \left(-\omega^2 \left(\mathbf{A}_j\right)_{\bullet q_j} + \mathrm{i}\omega \left(\mathbf{B}_j\right)_{\bullet q_j}\right) + \mathbf{G}_j \boldsymbol{a}_j^I & i = j \end{cases} \tag{15}$$

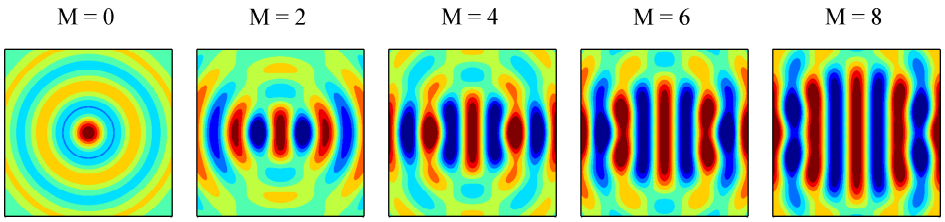

Figure 1: Incident plane wave as a summation of partial cylindrical waves (equation 2), plotted as the surface elevation, $\mathrm{Re}\left\{-(\mathrm{i}\omega/g)\,\phi^P\big|_{z=0}\right\}$, for increasing truncation values, M.

where $\left(\mathbf{F}_i^R\right)_{\bullet q_j}$ is the q_j^{th} column of the radiation force matrix on body i, $\mathbf{F}_i^R$, and $(\mathbf{A}_j)_{\bullet q_j}$ and $(\mathbf{B}_j)_{\bullet q_j}$ are the q_j^{th} column vector of the added mass and damping matrices of body j in isolation. $\mathbf{F}_i^R$ is $Q_i \times Q$ matrix, and the radiation force matrix for the complete system of bodies is

$$\mathbf{F}^R = \begin{bmatrix} \mathbf{F}_1^R \\ \mathbf{F}_2^R \\ \vdots \\ \mathbf{F}_N^R \end{bmatrix} \tag{16}$$

where the added mass and damping matrices of the entire system of bodies are given by $\mathbf{A} = -\frac{1}{\omega^2}\mathrm{Re}\left\{\mathbf{F}^R\right\}$ and $\mathbf{B} = \frac{1}{\omega}\mathrm{Im}\left\{\mathbf{F}^R\right\}$.

3. Derivations of the Diffraction Transfer and Force Transfer Matrices

The diffraction transfer matrix is a linear operator representing a body that transforms an incident wave into a scattered wave. Historically it has not been widely used, because the incident and scattered waves are of a somewhat unusual forms - infinite summations of cylindrical partial waves. Figure 1 helps to illustrate how cylindrical partial waves can represent an incident plane wave. It shows the incident wave computed with its cylindrical representation, (equation 2), for increasing truncation values, M. At $M = 0$, the pattern looks like a wave due to a heaving body, but with increasing M, the wave becomes more and more plane-wave-like in the region of the

origin. For the scattered wave, the cylindrical solution is a very natural representation as discussed by McNatt et al. (2013).

Previously, each component of the diffraction transfer matrix, D_{mn}, was derived by solving the scattering BVP to find the m^{th} scattered wave coefficient due to an incident cylindrical wave component, n. This has been performed analytically for cylinders (Yilmaz, 1998), and computationally in a BEM with cylindrical Green functions (Goo and Yoshida, 1990). Note that a commercial BEM with cylindrical Green functions is not available, and in-house coding is difficult. The primary aim of this work is to enable the interaction theory of Kagemoto and Yue (1986) by developing a method to find the diffraction transfer matrix with commonly available means.

In the following sections, it is shown how the diffraction transfer matrix as well as the force transfer matrix can be derived from numerical or physical measurements from a series of incident plane waves at directions from 0 to 2π. First, a method is described to find the scattered wave coefficients due to an incident wave (only later is the incident wave assumed to be plane), and to find the radiated wave coefficients. Then, the method is applied successively to plane waves at different incident wave directions to the body to find the diffraction transfer matrix. The force transfer matrix is then found with an analogous technique.

3.1. Derivation of the cylindrical wave coefficients

Now including evanescent modes, the complete linear-wave solution to the BVP for the scattered and radiated waves of body i in the fluid domain outside of the body is

$$\phi_i^{S,R} = \mathrm{i}\frac{\mathrm{g}}{\omega} \sum_{m=-\infty}^{\infty} \left(\boldsymbol{\chi}_i^{S,R}\right)_m e^{\mathrm{i}m\theta_i} \tag{17}$$

$$\begin{aligned}\left(\boldsymbol{\chi}_i^{S,R}\right)_m = &\left(\boldsymbol{a}_i^{S,R}\right)_m \frac{\cosh k_0\left(h+z\right)}{\cosh k_0 h} H_m^{(2)}\left(k_0 r_i\right) \\ &+ \sum_{l=1}^{\infty} \left(\boldsymbol{b}_i^{S,R}\right)_{lm} \cos k_l\left(h+z\right) K_m\left(k_l r_i\right)\end{aligned} \tag{18}$$

where $\boldsymbol{a}_i^{S,R}$ is again the vector of scattered or radiated propagating wave coefficients (as in Sec. 2.1). $\boldsymbol{b}_i^{S,R}$ is a vector of evanescent wave coefficients, whose lm^{th} value is the amplitude of the partial wave of due to evanescent

mode l, corresponding the evanescent wave number, k_l, and circular mode m, and K_m is the m^{th} order modified Bessel function of the second kind.

$\left(\boldsymbol{\chi}_i^{S,R}\right)_m$ can be found as the Fourier transform of the velocity potential,

$$\left(\boldsymbol{\chi}_i^{S,R}\right)_m = -\frac{\mathrm{i}}{2\pi}\frac{\omega}{g}\int_0^{2\pi}\phi_i^{S,R}e^{-\mathrm{i}m\theta_i}d\theta_i \tag{19}$$

By substitution of the propagating and evanescent mode dispersion relations and integration, the depth dependencies can be shown to be orthogonal,

$$\int_{-h}^{0}\cosh k_0\left(h+z\right)\cos k_l\left(h+z\right)dz = 0 \tag{20}$$

$$\int_{-h}^{0}\cos k_l\left(h+z\right)\cos k_n\left(h+z\right)dz = 0,\ l\neq n \tag{21}$$

which means that integration of $\left(\boldsymbol{\chi}_i^{S,R}\right)_m$ over depth can be used to isolate the propagating or evanescent partial waves.

For either the scattering or the radiation problem, if the potential, $\phi_i^{S,R}$, is known over a cylindrical surface encompassing the body that extends from the bottom to the mean free surface at a constant radius $r_i = R_i$, the propagating and evanescent wave coefficients can be found by integration over the cylindrical surface,

$$\begin{aligned}\left(\boldsymbol{a}_i^{S,R}\right)_m =& -\frac{\mathrm{i}}{2\pi}\frac{\omega}{g}\frac{2\cosh k_0 h}{h\left(1+\frac{\sinh 2k_0h}{2k_0h}\right)}\frac{1}{H_m^{(2)}\left(k_0R_i\right)}\\ &\times\int_{-h}^{0}\int_0^{2\pi}\phi_i^{S,R}\left(R_i,\theta_i,z\right)e^{-\mathrm{i}m\theta_i}\cosh k_0\left(h+z\right)d\theta_i dz\end{aligned} \tag{22}$$

$$\begin{aligned}\left(\boldsymbol{b}_i^{S,R}\right)_{lm} =& -\frac{\mathrm{i}}{2\pi}\frac{\omega}{g}\frac{2}{h\left(1+\frac{\sin 2k_lh}{2k_lh}\right)}\frac{1}{K_m\left(k_lR_i\right)}\\ &\times\int_{-h}^{0}\int_0^{2\pi}\phi_i^{S,R}\left(R_i,\theta_i,z\right)e^{-\mathrm{i}m\theta_i}\cos k_l\left(h+z\right)d\theta_i dz\end{aligned} \tag{23}$$

The velocity potential over a cylindrical surface can be derived by any computational method or by experiments, as long as linearity of the problem is given or assumed. Further details on the computation of the coefficients is given in McNatt et al. (2013).

3.2. The diffraction transfer matrix from incident plane waves

For an incident propagating plane wave at a direction β_n, the cylindrical propagating scattered wave coefficients, $\boldsymbol{a}_i^S(\beta_n)$ can be computed as described above. For which, the diffraction transfer matrix solves the equation:

$$\boldsymbol{a}_i^S(\beta_n) = \mathbf{D}_i \boldsymbol{a}_i^P(\beta_n) \tag{24}$$

$\boldsymbol{a}_i^P(\beta_n)$ is known and is given by equation 3, $\boldsymbol{a}_i^S(\beta_n)$ is found by the procedure in section 3.1. $\mathbf{D}_i$ is a matrix of unknown elements. For a single wave direction, equation 24 is an under-determined matrix equation. Using the truncation value, M_i, the incident and scatter coefficient matrices are vectors of length $2M_i+1$, and diffraction matrix is of size $(2M_i+1)\times(2M_i+1)$. To find $\mathbf{D}_i$, $2M_i$ more equations are needed.

The additional equations are produced by solving for the scattered coefficients for at least $2M_i$ more wave directions going from 0 to 2π. By calling the vector of incident wave directions $\boldsymbol{\beta}$, $\left[\boldsymbol{a}_i^S(\boldsymbol{\beta})\right]$ is a matrix whose value at the m^{th} row and n^{th} column is the scattered wave coefficient of the m^{th} partial wave due to an incident wave in the direction β_n. Similarly, $\left[\boldsymbol{a}_i^P(\boldsymbol{\beta})\right]$ is a matrix whose value at the m^{th} row and n^{th} column is the incident regular wave amplitude given by equation 3. With this, equation 24 become a full matrix equation

$$\left[\boldsymbol{a}_i^S(\boldsymbol{\beta})\right] = \mathbf{D}_i \left[\boldsymbol{a}_i^I(\boldsymbol{\beta})\right] \tag{25}$$

$\left[\boldsymbol{a}_i^S(\boldsymbol{\beta})\right]_{m\bullet}$ is the m^{th} row vector of $\left[\boldsymbol{a}_i^S(\boldsymbol{\beta})\right]$ - the scattered wave coefficients of circular mode m for different incident wave directions. The m^{th} row of the diffraction transfer matrix, $(\mathbf{D}_i)_{m\bullet}$, can be found by solving the system of equations:

$$\left[\boldsymbol{a}_i^S(\boldsymbol{\beta})\right]_{m\bullet}^{\mathsf{T}} = \left[\boldsymbol{a}_i^P(\boldsymbol{\beta})\right]^{\mathsf{T}} (\mathbf{D}_i)_{m\bullet}^{\mathsf{T}} \tag{26}$$

Only $2M_i+1$ incident wave directions are needed to solve for a diffraction transfer matrix of size $(2M_i+1)\times(2M_i+1)$. However, it was found to be more accurate to compute scattered wave coefficients for greater than $(2M_i+1)$ incident directions to create an over determined system and then fit row vectors $(\mathbf{D}_i)_{m\bullet}$.

For a given incident plane wave, one can also compute the scattering coefficients, $\boldsymbol{b}_i^S$, of the evanescent wave modes. To use the evanescent mode in the interaction problem, one would need to find scattering coefficients due to

incident evanescent waves. However, incident partial evanescent wave modes do not exist in isolation and so would be challenging to create experimentally or with nonlinear computational software, and they are not included in commercial linear wave software. The derivation of a diffraction transfer matrix that includes evanescent wave modes is not practical experimentally or computationally following the method given here.

Here the diffraction transfer matrix is found by probing the body with incident plane waves from different directions. In the BEM of Goo and Yoshida (1990) and Chakrabarti (2000), the diffraction transfer matrix was found by probing the body directly with incident cylindrical waves. To find column n of $\mathbf{D}_i$, the n^{th} order incident cylindrical wave was used (each row m was found by using the m^{th} order cylindrical Green function). So for the same truncation value, M_i, the method presented here for determining the diffraction transfer matrix from plane waves requires the same number of incident waves (except where accuracy is improved by overdetermining the system) as methods that directly use incident cylindrical waves.

3.3. The force transfer matrix from incident plane waves

In a manner analogous the derivation of the diffraction transfer matrix, the force transfer matrix of body i, $\mathbf{G}_i$, can be found by computing the forces on body i due to multiple incident wave directions $\boldsymbol{f}_i(\beta_n)$. $\boldsymbol{f}_i(\beta_n)$ is a $Q_i \times 1$ vector. $\mathbf{G}_i$ is a $Q_i \times (2M_i + 1)$ matrix. Like the diffraction transfer matrix, one finds $\mathbf{G}_i$ by solving for a vector of different incident wave directions, $\boldsymbol{\beta}$, where the number of wave directions is at least but preferably greater than $2M_i + 1$.

$$[\boldsymbol{f}_i(\boldsymbol{\beta})] = \mathbf{G}_i \left[\boldsymbol{a}_i^P(\boldsymbol{\beta})\right] \tag{27}$$

The q_i^{th} row of the matrix,$[\boldsymbol{f}_i(\boldsymbol{\beta})]_{q_i\bullet}$, represents the forces on mode q_i at each incident wave direction. The q_i^{th} row of the force transfer matrix can be solved as

$$[\boldsymbol{f}_i(\boldsymbol{\beta})]_{q_i\bullet}^{\mathsf{T}} = \left[\boldsymbol{a}_i^P\left(\boldsymbol{\beta}^{\mathsf{T}}\right)\right]^{\mathsf{T}} (\mathbf{G}_i)_{q_i\bullet}^{\mathsf{T}} \tag{28}$$

3.4. Rotation of the body

In some cases for an interaction computation, a body in the array may be rotated with respect to the orientation for which its diffraction transfer and force transfer matrices were computed. This does not present a problem,

and a rotation was shown originally by Peter and Meylan (2004). A body rotation is akin to a redefining the body coordinate system. For the rotation of the diffraction transfer matrix, this must be done for the scattered wave amplitudes as well as the incident wave amplitudes.

Consider the rotation angle γ_i of body i, the modified scattered basis function is

$$\begin{aligned}\left(\boldsymbol{\Psi}^S_{i,\gamma_i}\right)_m &= \frac{\cosh k_0\left(h+z\right)}{\cosh k_0 h} H^{(2)}_m\left(k_0 r_i\right) e^{\mathrm{i}m(\theta_i-\gamma_i)} \\ &= e^{-\mathrm{i}m\gamma_i}\left(\boldsymbol{\Psi}^S_i\right)_m \end{aligned} \tag{29}$$

which is the product of $e^{-\mathrm{i}m\gamma_i}$ and the standard basis function. The same rotation applies to the incident basis function. Applying this to the diffraction transfer matrix relationship:

$$\begin{aligned} e^{-\mathrm{i}m\gamma_i}\left(\boldsymbol{a}^S_i\right)_m &= \left(\mathbf{D}_i\right)_{mn} e^{-\mathrm{i}n\gamma_i}\left(\boldsymbol{a}^I_i\right)_n \\ \left(\boldsymbol{a}^S_i\right)_m &= e^{\mathrm{i}(m-n)\gamma_i}\left(\mathbf{D}_i\right)_{mn}\left(\boldsymbol{a}^I_i\right)_n \end{aligned} \tag{30}$$

Clearly, $e^{\mathrm{i}(m-n)\gamma_i}$ is the adjustment of diffraction transfer coefficient $\left(\mathbf{D}_i\right)_{mn}$ due to a body rotation, γ_i.

For the force transfer matrix, the situation is a simpler, only the incident waves need to be rotated, $\boldsymbol{f}_{i,\gamma_i} = e^{-\mathrm{i}m\gamma_i}\left(\mathbf{G}_i\right)_{\bullet m}\left(\boldsymbol{a}^I_i\right)_m$. Similarly, the radiation coefficients must be rotated by $e^{-\mathrm{i}m\alpha\gamma_i}$. The complete set of rotations is then

$$\left(\mathbf{D}_{i,\gamma_i}\right)_{mn} = e^{\mathrm{i}(m-n)\gamma_i}\left(\mathbf{D}_i\right)_{mn} \tag{31}$$

$$\left(\mathbf{G}_{i,\gamma_i}\right)_{\bullet m} = e^{-\mathrm{i}m\gamma_i}\left(\mathbf{G}_i\right)_{\bullet m} \tag{32}$$

$$\left(\boldsymbol{a}^R_{q_i,\gamma_i}\right)_m = e^{-\mathrm{i}m\gamma_i}\left(\boldsymbol{a}^R_{q_i}\right)_m \tag{33}$$

Thus the diffraction transfer matrix and force transfer matrix have been derived and their application has been shown for the computation of excitation forces and added mass and damping matrices on arrays of floating bodies.

4. Summary of computational procedures

The preceding theory is long and complex, and so it helps to have the computational steps summarized in the order they are applied. The following quantities need to be computed for each unique geometry in isolation prior to solving the interaction problem.

1. *Standard linear hydrodynamic properties* - For each unique geometry in isolation, one needs to compute the added mass, damping, and hydrostatic matrices.
2. *The force transfer matrix* - Excitation forces are found for each mode of motion due to incident plane waves for at least M_i directions from $0 - 2\pi$. Body symmetry can be exploited to reduce the number of directions required. These forces are used derive the force transfer matrix as in section 3.3.
3. *The diffraction transfer matrix* - Each scattered wave field is measured over a cylindrical surface surrounding the body due to incident plane waves for at least M_i directions from $0 - 2\pi$. Body symmetry can be exploited to reduce the number of directions required. These measured points are used to compute the diffraction transfer matrix as in sections 3.1 and 3.2.
4. *Radiated wave coefficients* - For each mode of motion, wave field points are measured over a cylindrical surface surrounding the body due to unit-amplitude forced motion. These measured points are used to compute the radiated wave coefficients for each mode of motion as in section 3.1.

Once these hydrodynamic quantities have been found, they can be used in the interaction theory to find the hydrodynamic quantities for an array of bodies.

1. *Rotate bodies* - If any of the bodies in the interaction problem are rotated relative to the orientation at which their hydrodynamic quantities were computed, the hydrodynamic quantities are modified as in section 3.4.
2. *The scattering problem* - The scattering problem is used to find the excitation forces for the entire array. First the scattering problem is solved as in section 2.2, where the ambient incident wave is a plane wave at the direction of interest. Next the excitation force on each body is found with the force transfer matrix as in section 2.3.1.

3. *The radiation problem* - The radiation problem is used to find the added mass and damping matrices for the entire array. For each mode of motion in the array, a scattering problem is solved (section 2.2), where the ambient incident wave is the wave radiated by that mode of motion. The added mass and damping matrices are assembled for the array following section 2.3.2.

The added mass, damping, and excitation forces for the array can then be used to calculate body motions and wave power absorption in the standard manner (e.g. see Cruz (2008)), where the matrices (added mass, damping, stiffness, etc.) and vectors (motions and forces) are taken to be those for the entire system. Results from the application of the method are shown and discussed in the next section and, where possible, are verified against direct method results computed with the BEM software WAMIT.

5. Results

In the results section, the interaction theory computational method is verified against the direct method computed with the commercial BEM software, WAMIT. Also presented are two cases where a direct BEM computation is not practical due to lengthy computation time, and which therefore can only be computed with interaction theory. Two geometries are considered - a floating cylinder and an attenuator-type WEC. Two array cases are examined for verification - two bodies at various distances, and a medium sized array of greater than 10 bodies. Finally, using only interaction theory, a computation is made on a medium-sized array of WECs in spectral seas, and on a very large array of 101 WECs in regular waves.

5.1. Geometries

The cylinder has a radius a, a height, $1.5a$, and a draft a (portion below the still water level). It is uniform in density and free to move in 6 degrees-of-freedom (1 - surge, 2 - sway, 3 - heave, 4 - roll, 5 - pitch, 6 - yaw) with no external mechanical forces applied. All values are non-dimensionalized by the cylinder radius, a. It is shown as its low-order panelization in figure 2-a. All computations are performed in a water depth of $h/a = 10$.

The attenuator-type WEC is sometimes called a hinged raft, whose performance was considered by Newman (1979). It consists of three cylindrical bodies hinged together to rotate about axes parallel to the y-axis. It has

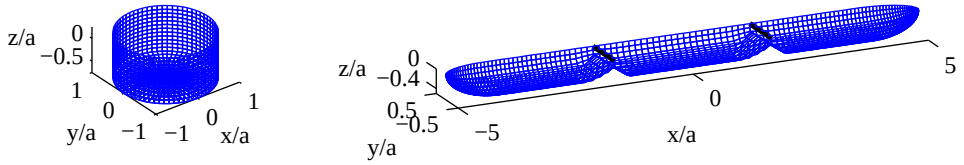

(a) Cylinder

(b) Attenuator

Figure 2: Cylinder and attenuator geometries shown as their panelization for the BEM computation. Black lines indicate attenuator hinges. All dimensions are nondimensionalized by the cylinder's radius, a.

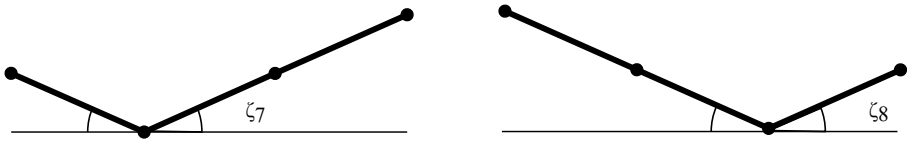

(a) Forward hinge motion

(b) Aft hinge motion

Figure 3: Diagram of definitions of hinged motions for attenuator. ζ_7 is 'Forward Flex', where the 'front' of the attenuator is taken to be the end which meets the waves first at an incident wave direction of $\beta = 0$. ζ_8 is 'Aft Flex'.

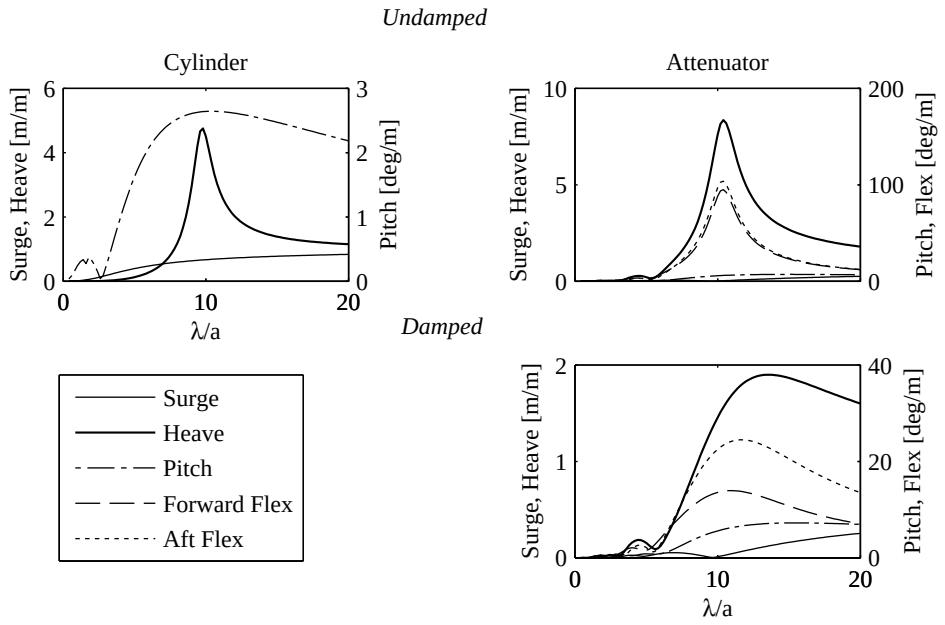

Figure 4: Cylinder and attenuator body motions as response amplitude operators as functions of nondimensional wavelength. Linear motions are shown on left-hand axes as meters of response per meter of incident wave amplitude, and rotational motions are shown on right-hand axes as degrees of response per meter of incident wave amplitude. Attenuator body motions are for head-seas ($\beta = 0$) and are shown for both damped and undamped case.

8 degrees-of-freedom - the same 6 rigid body motions as the cylinder and 2 'flex' motions (mode 7 is flex in the forward hinge, and 8 is flex in the aft hinge). A unit amplitude flex motion defined as shown in figure 3. It has a beam of a, and a total length of $10a$. Its ends are spheroidal; there are notches at the hinges; and it is semi-submerged - see figure 2-b.

The dimensions of both geometries where chosen so that each had resonant peaks in heave at $\lambda/a = 10$. The cylinder and attenuator motions as the response amplitude operator, $|\zeta_{q_i}/A|$, plotted as a function of non-dimensional wavelength are shown in figure 4. However, besides resonant peak condition, the dimensions of the geometries are arbitrary and the interaction theory method could be applied to any shape.

For the attenuator, motion of a given point in the geometry about hinge n, located at $\{x_n, z_n\}$, is described by the vector function $\boldsymbol{\zeta}_n$

$$\boldsymbol{\zeta}_n = |z - z_n| \operatorname{sign}(x - x_n)\, \mathbf{i} + |x - x_n|\, \mathbf{k} \tag{34}$$

where $\mathbf{i}$ and $\mathbf{k}$ are the unit vectors in the body x and z directions respectively. The hinge positions of the attenuator in body coordinates are: $\{x_7, z_7\} = \left\{-\frac{5}{3}, 0\right\}$, and $\{x_8, z_8\} = \left\{\frac{5}{3}, 0\right\}$.

The flex motions are coupled ineritially to one another and to surge, heave, and pitch. The mass matrix is computed following Newman (1977, Sec. 4.16), $(\mathbf{M})_{ij} = \int\int\int \boldsymbol{\zeta}_i \cdot \boldsymbol{\zeta}_j dm$. More information on hinge modes can also be found in Newman (1997). Due to the coupling between the heave and flex modes, the WEC develops an interesting resonance in the heave-flex motion. For mechanically undamped motion, the linear computation leads to unrealistic motions. Figure 4 shows the motions of the attenuator for normally incident waves with no external mechanical forces. To reduce the resonance and make the WEC motions more realistic (i.e. not as extreme), the power take-off damping is not the optimal value leading to maximum theoretic power absorption, but still resulted in a reasonable power capture.

5.2. Excitation force and radiation values

In this section, excitation force and radiation values for an array of two bodies are considered as a function of body separation distance, d/a, at three wavelengths: $\lambda/a = 3, 10, 30$, and a constant water depth of $h/a = 10$. Three incident wave directions are considered for the excitation force computation: $\beta = 0,\ \frac{\pi}{4},\ \frac{\pi}{2}$.

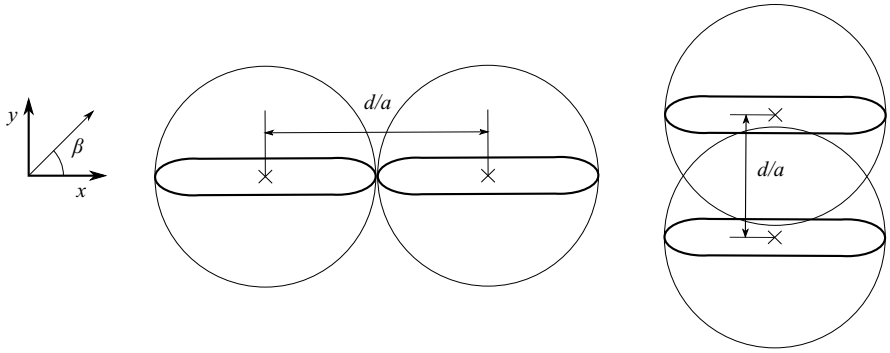

Figure 5: Two arrangements of the attenuator for the distance verification computation. The outline of the attenuator is shown as the thick line; it origin is given by the 'x'; and its circumscribing cylinder is given by the thin line. By the interaction theory, the center of one body must be outside of the circumscribing cylinder of the other body.

The separation distance is the origin-to-origin distance between the geometries. The cylinders are aligned along the x-axis. Due to the axisymmetry of the cylinder, only the separation distance needs be considered; body orientation is irrelevant. However, for the attenuator pairs, there are three parameters - body separation, direction of separation, and the relative orientation of the second body to the first. For the separation analysis - two cases were considered: 1) two attenuators, parallel in orientation, and set up in-line and front to back and 2) two attenuators, parallel in orientation, and set side by side. These arrangements can be seen in figure 5. A restriction imposed by Graf's addition theorem is that the center of the second body must be outside the circumscribing circle of the first body and vice versa. For the front to back orientation, even though the bodies themselves are closer (nearly touching at the minimum distance), the body spacing in terms of interaction theory is in fact further than for the side by side case.

The only theoretical difference between the results of the interaction theory computation and WAMIT is the absence of evanescent waves in the interaction theory. The effect should only be present at small separation distances.

For each of the layouts, all of the excitation force values and all important added mass and damping values were examined. The agreement in almost

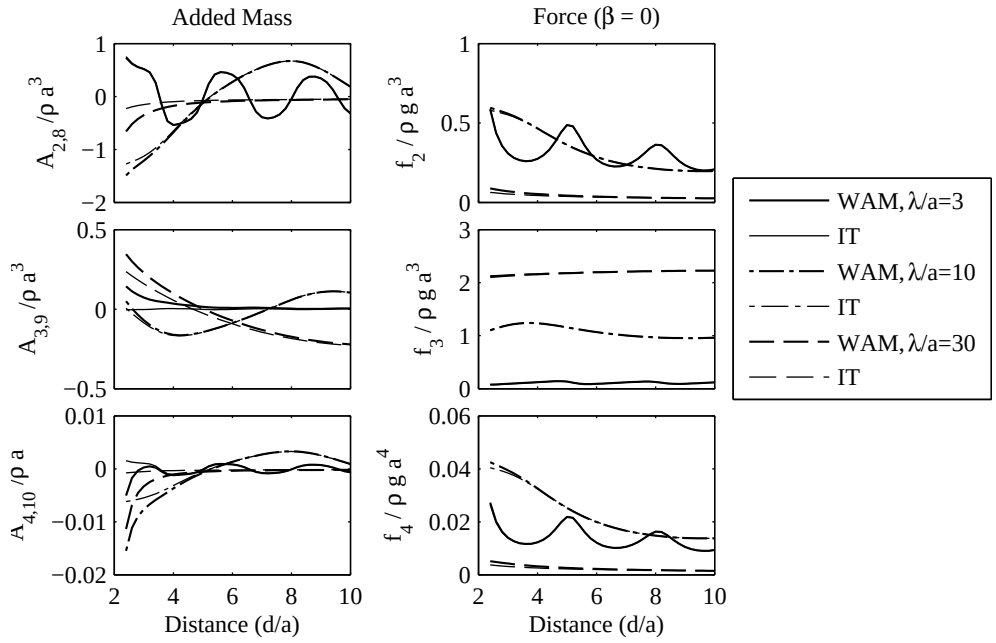

Figure 6: Plots of added mass ($\boldsymbol{A}$) and excitation force ($\boldsymbol{f}$) for plane incident waves at a direction $\beta = 0$ for two cylinders as a function of nondimensional separation distance. Subscripts $1-6$ are the six DOFs of the first body, and subscripts $7-12$ are the 6 DOFs of the second body. For example, $A_{2,8}$ is the added mass of sway-sway coupling between the bodies. WAM - WAMIT computation; IT - interaction theory computation.

all cases was excellent with the only differences being found at short separation distances. Example plots, selected because they show some of the largest disagreement, are given for the cylinders in figure 6 and for the attenuators in figure 7. The benchmark WAMIT computations are represented as think lines, and the interaction theory computations are thin lines. In some figures, only thick lines are visible, which means that the interaction theory computation line is beneath it and the computations are in excellent agreement. For the cylinder computation, one can see differences between the two computations at short distances due to the evanescent wave effects, particularly so in the added mass. For the attenuator in the front to back configuration, one also sees evanescent wave effects at short distances. In both of these cases, the two bodies are almost touching.

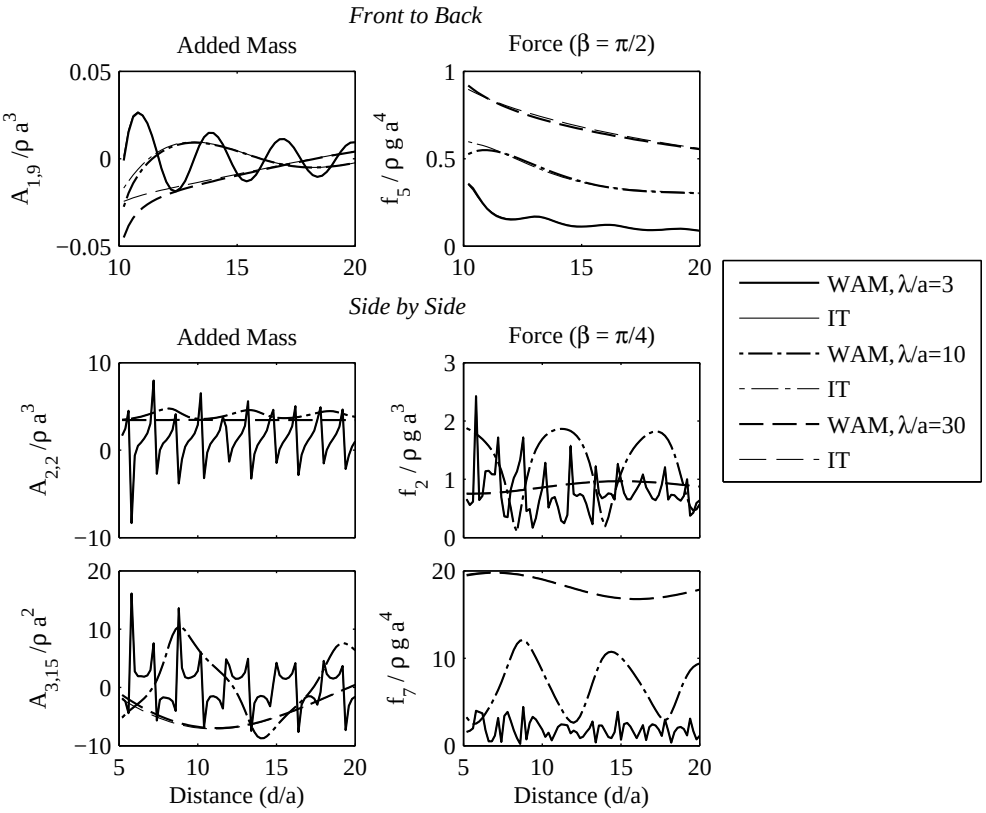

Figure 7: Plots of added mass ($\boldsymbol{A}$) and excitation force ($\boldsymbol{f}$) for plane incident waves for two attenuators as a function of nondimensional separation distance in the Front-to-Back and Side-by-Side arrangements (see figure 5). Subscripts $1-8$ are the six standard DOFs plus the two flex modes of body one, and subscripts $9-16$ are the 8 DOFs of the second body. For example, $A_{3,15}$ is the added mass of heave-'forward flex' coupling between the bodies. WAM - WAMIT computation; IT - interaction theory computation.

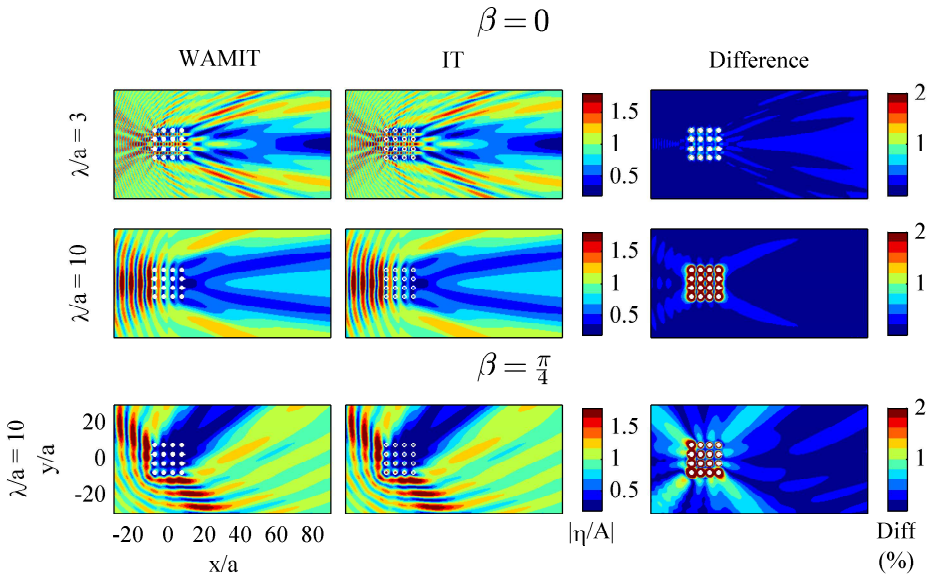

Figure 8: The figures show wave fields produced with WAMIT and the interaction theory (IT) computations, plotted as the magnitude of surface elevation, $|\eta| = |-(\mathrm{i}\omega/g)\,\phi|_{z=0}|$, at two nondimensional wavelengths and for two incident wave directions, for an array of 16 cylinders. Also shown is the percentage difference between the wave fields, $100\% \times |\eta_{IT} - \eta_{WAM}|$.

5.3. Medium sized arrays

In this section, the interaction theory computation is verified by examining the wave fields of medium sized arrays. The wave field is plotted as the magnitude of the total wave elevation normalized by the incident wave amplitude, $|\eta/A|$, which centers the value around 1. The total wave elevation is the sum of the incident, scattered, and radiated wave elevations, and inherently includes the effects of the computed body motions. Also shown is 100 times absolute value of the difference between the wave fields: $100 \times \left|\left(\eta^{IT} - \eta^{WAM}\right)/A\right|$, which can be thought of as a percentage difference relative to the incident wave amplitude.

Figure 8 shows the results for an array of 16 cylinders in a square 4×4 grid, with a spacing of $d/a = 5$. In general, for all wave fields there is very good agreement. The difference is less than 0.2% for most of the wave fields. At $\lambda/a = 10$, $\beta = 0$, one can see differences in the wave fields near the cylinders themselves resulting from the evanescent waves (at a distance of

$1a$ from the wall of any given cylinder, the difference is less than 4%). This difference dies out in the far-field wave field. In contrast at $\lambda/a = 10$, $\beta = \frac{\pi}{4}$, there is a small difference that propagates into the far-field. At this incident wave angle, some of the heave body motions are larger than at $\beta = 0$, which results in larger radiated evanescent waves and leads to differences in the body motions.

Figure 9 shows the results for an array of 11 attenuator WECs, setup in two offset rows. The bodies are shown as well as the circumscribing circle from which the cylindrical coefficients were computed. One would not expect agreement in the wave fields inside this circle. The center to center distance between bodies in a row is $d/a = 20$, and the row spacing is $d/a = 20$. At an incident direction, $\beta = \pi/4$, the front row of bodies has been rotated to demonstrate the calculation described in section 3.4. At this spacing evanescent wave effects are non-existent and the agreement between the wave fields for all conditions is excellent (generally less than a 0.2% difference).

5.4. Spectral Array

In this section, a spectral wave field is considered. The incident sea spectrum is a Bretschneider spectrum with a peak at a wavelength, $\lambda/a = 10$, and a cosine-squared spreading, $D(\theta) = A_2 \cos^{2s}\left(\frac{1}{2}\theta\right)$, where A_2 is the normalizing constant and $s = 10$ (Holthuijsen, 2007). 24 frequency components and 5 directions were implemented for a total of 120 wave components. The computation time for the array with this many wave components would be very long using the direct method, and so it was only be performed using interaction theory.

For WEC arrays, a common measure of the impact of the array effects on device performance is the interaction factor. Although it has slightly varying definitions throughout literature, here it is defined for a single WEC in the array, i, as ratio of power absorbed by that WEC to the power absorbed by the same single WEC in isolation - $q_i = \frac{P_i}{P_{isolated}}$. For the attenuator, the power absorbed is the total power for both hinges over all incident wave frequencies and directions. A q greater than 1 indicates that the given WEC performs better due to array effects, and conversely, for q less than one, the WEC performs worse.

Figure 10 shows the interaction factor and the wave field for the 11 WEC array in spectral seas. The wave field is plotted as the disturbance coefficient - the ratio of significant wave height at a field point to the incident significant wave height $\left|H_s/H_s^I\right|$. The interaction factor shows that the front row of

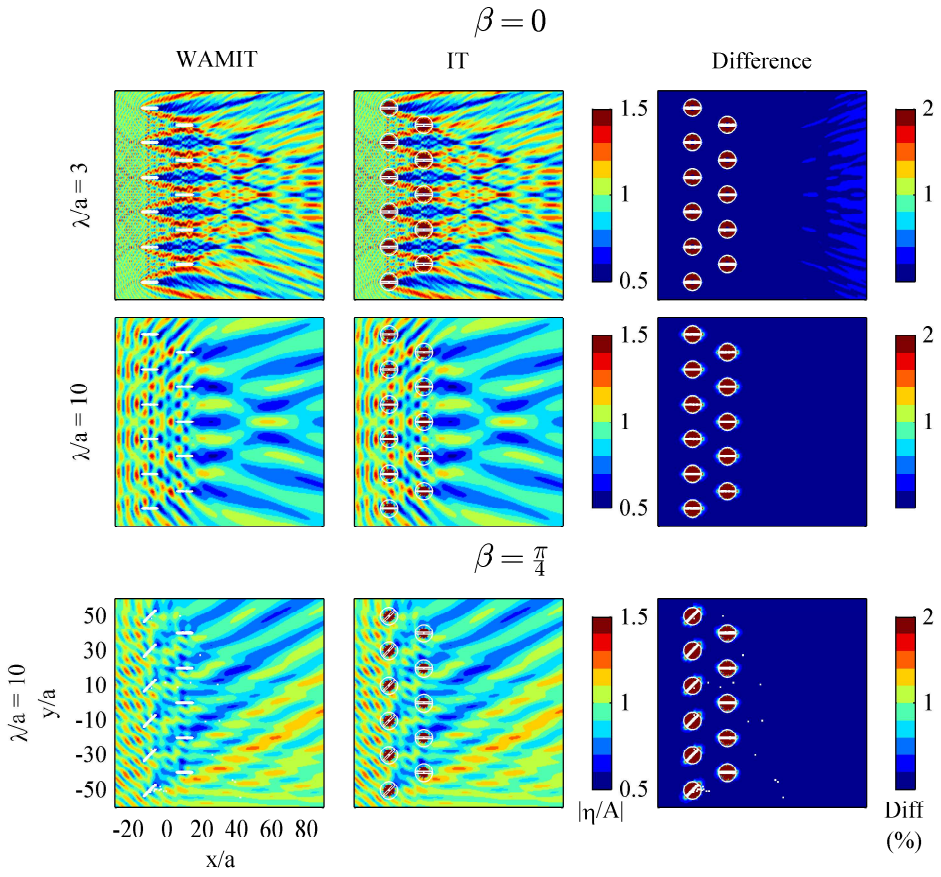

Figure 9: The figures show wave fields produced with WAMIT and the interaction theory (IT) computations, plotted as the magnitude of surface elevation, $|\eta| = |-(\mathrm{i}\omega/g)\ \phi|_{z=0}|$, at two nondimensional wavelengths and for two incident wave directions, for the 11 attenuator array. Also shown is the percentage difference between the wave fields, $100\% \times |\eta_{IT} - \eta_{WAM}|$. At $\beta = \frac{\pi}{4}$, the front row of attenuators is rotated to face the incident waves to demonstrate the rotation given in section 3.4.

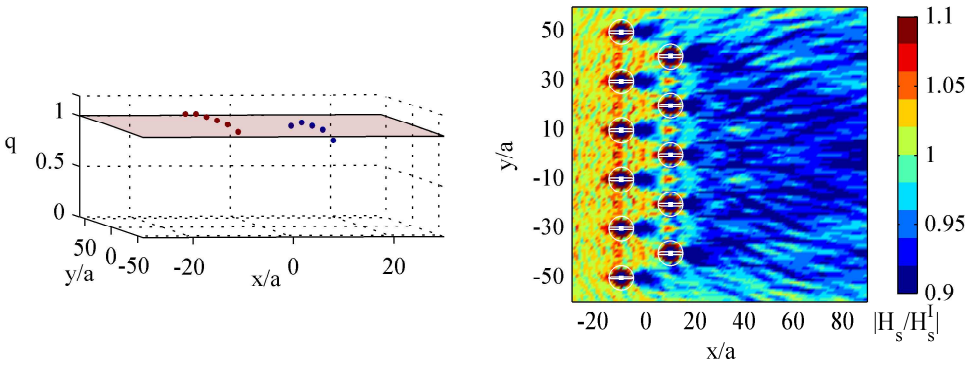

(a) Interaction factor

(b) Wave field

Figure 10: The plots are for the 11 attenuator array in spectral seas. Figure (a) shows the interaction factor, q, for each body as a function of its position. q is a measure of the effect of multi-body interactions on power absorption. Figure (b) shows the wave field for as the disturbance coefficient, $\left|H_s/H_s^I\right|$.

WECs receives a slight boost in performance (+3% to +7%), likely due to reflection of waves from the rear row. The performance of the rear row is slightly diminished (-0.5% to -7%) due to wave shadowing from the front row. The wave field shows wave energy reflection in front of the WECs and a wave shadow behind the array.

5.5. Large WEC Array

In this section, an example of a very large WEC array of 101 bodies (808 degrees-of-freedom) is computed for a regular wave: $\lambda/a = 10$ at $\beta = 0$. The array is divided into 3 rows and the spacing between WECs in a row and between rows is $d/a = 20$. To the authors' knowledge no computations of arrays this large have been made with the direct method due to the limitations of today's computational resources.

Results for the very large WEC array are shown in figure 11. The interaction factor results are interesting and somewhat unintuitive - it shows that the performance of the first two rows is reduced by the array effects, but the power performance of the final row is actually increased. One would expect the opposite, as was seen for the spectral array. However, at individual frequencies, the coherent interaction between the incident wave and scattered and radiated waves, creates standing waves, which act to increase or reduce wave energy at localized points in the wave field. Performance

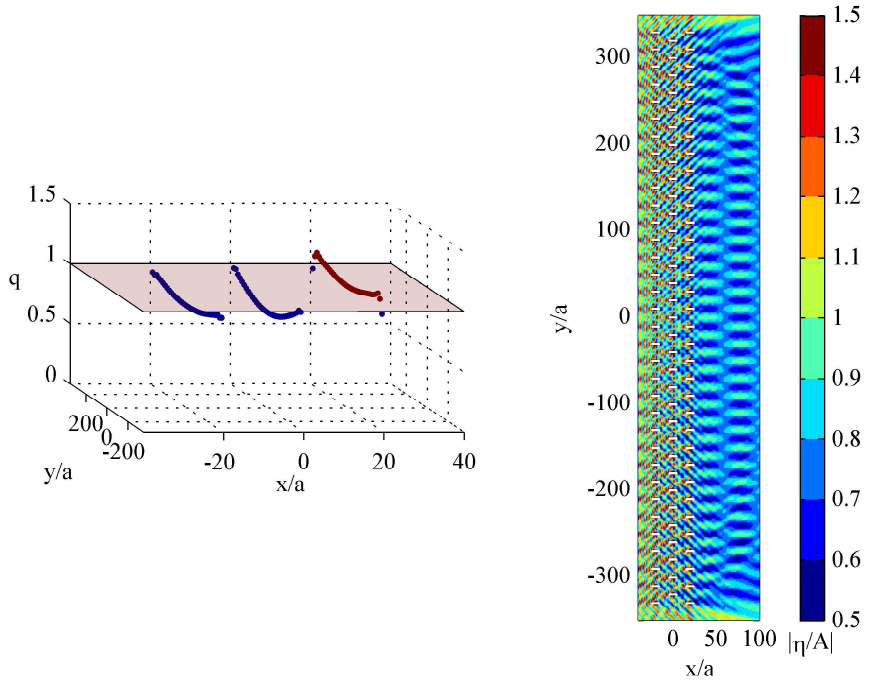

(a) Interaction factor

(b) Wave field

Figure 11: The plots are for the 101 attenuator array in regular waves, $\lambda/a = 10$, $\beta = 0$. Figure (a) shows the interaction factor, q, for each body as a function of its position. q is a measure of the effect of multi-body interactions on power absorption. Figure (b) shows the wave field, as the magnitude of wave elevation, $|-(\mathrm{i}\omega/g)\ \phi|_{z=0}|$.

gains or losses due to these standing wave effects are very sensitive to the ratio of wavelength to body spacing. The effects shown here should not be generalized, but serve to dispel the beliefs that the effects on back rows are always negative and that no more than two rows of WECs should be used in an array.

6. Discussion

The purpose of interaction theory is to accelerate the linear hydrodynamic computation of arrays without losing accuracy. The method developed herein enables the interaction theory calculation with minimal requirements for complex custom software development. With that in mind, it is important to first consider the extent of the computational acceleration and why

it results. After which, shortcomings of the method, including the absence of evanescent waves, the flat bottom condition, and the long-crested incident wave, are discussed and their significance assessed.

The most time-consuming computation in both the direct BEM and the interaction theory calculations is the solution to the resulting system of linear equations. For interaction theory the system is given by equation 12. Solving a system of equations using an iterative method leads to a computation time of $O\left(L^2\right)$, where L is the number of unknowns (Newman and Lee, 2002). For the low-order BEM, the number of unknowns is equal to the total number of panels in the system. For an array of N identical bodies, each with P panels, the total number of unknowns is NP, and the computation time is $O\left(N^2P^2\right)$.

For the interaction theory, the number of unknowns is equal to the number of scattered wave modes included in the problem. The number of scattered waves is determined by the cylindrical partial-wave truncation value, M, where the number of scattered waves is $2M+1$. For an array of N identical bodies, the total number of unknowns is $N\left(2M+1\right)$and the computation time is $O\left(N^2\left(2M+1\right)^2\right)$. Herein, the truncation value is determined based on the accuracy and precision of the measured wave field values used to compute the cylindrical wave field coefficients (section 3.1). M was determined as the point where all coefficients beyond M where smaller than the designated accuracy/precision floor of the wave field measurements used to determine the diffraction transfer matrix. For example, WAMIT returns field points to 6 significant figures. In computing the partial wave amplitudes (equation 22) with other software, these 'measurements' are padded with zeros, and the FFT returns values at accuracies greater than that of the original measurement, which of course are not real. Additionally, it was found that these phantom accuracies adversely affect computational results, and all the coefficients should be rounded to the accuracy/precision floor.

The number of panels and the number of scattered waves used for the cylinder and attenuator geometries is shown in table 1. In all cases, the number of geometry panels is two orders of magnitude greater than the number of scattered waves. Consider the attenuator at a wavelength of $\lambda/a = 10$, the number of panels is 1920, and the number of scattered waves is 25, which means that for a given array computation, regardless of the number of bodies, the direct method will take on the order of $\left(1920/25\right)^2$ (about 5900) times longer to compute. There is an upfront computational cost to the interaction theory computation. To compute the diffraction transfer matrix, force

		Cylinder	Attenuator
Panels (P)		1280	1920
	$\lambda/a = 3$	17	47
Scattered Waves	$\lambda/a = 10$	9	25
$(2M+1)$	$\lambda/a = 30$	9	15

Table 1: Panel and scattered wave count for each geometry

transfer matrix, and radiation wave field coefficients - values must be found at field points for $20-100$ incident wave directions on a single body for each wave frequency and water depth. However, once those quantities are found, they can be reused to drastically speed up array computations.

Here a few representative computation times are given. Both the WAMIT and interaction theory computations were performed on a desktop computer with a 3.3 GHz processor. WAMIT is written in Fortan and the interaction theory routine was coded in MATLAB (MATLAB R2013a, 2013) and uses the built-in 'mldivide' routine to solve the system of linear equations. No significant consideration was given to speeding up computation time for either the direct method or the interaction computation via parallel processing or other techniques. The following values should only be taken as rough estimates. A spectral computation as performed in section 5.4 leads to a linear increase in the computation time for both interaction theory and the direct method. With interaction theory, the spectral solution wave found for the entire array at all 24 frequencies and 5 wave directions in approximately 8 minutes. However using the direct method, it took roughly 40 minutes to find the the array solution at a single frequency and direction. For the very large array of 101 WECs each with 8 degrees-of-freedom, the interaction theory computation at a single wave frequency and direction took about 40 minutes. No equivalent computation was made with the direct method, although based on the computation with 11 bodies, theory suggests that the computation time for such an array would be about $2-3$ days.

In essence what interaction theory expresses is that to compute the linear-wave forces on an array of floating bodies, a detailed representation of each body is not needed; one only needs to know the shape, magnitude and phase of the waves it scatters. As solutions to the BVP, linear waves have a somewhat limited functional representation (i.e. sinusoidal), and so the scattered wave can be described by far fewer variables than are generally used to de-

scribe a geometric shape in BEM computation. Additionally, it was noticed that near the body, higher-order coefficients ($\left(\boldsymbol{a}_i^S\right)_m$ at large m values), even with very small amplitudes, were important to computations due to the exponential nature of the Hankel function, but far from the body the impact of the coefficients decayed exponentially with the Hankel function. So, even fewer partial cylindrical waves are required to compute bodies that are spaced far apart, and in essence as the distance from the body increases, the propagating wave effectively become more circular in shape.

The scattered wave solutions are only valid for the region outside the body. Underneath or on-top-of the body, another solution is required, for which the BEM is appropriate. A somewhat stricter limitation is imposed by the interaction theory computation. Due to restrictions in Graf's addition theorem, the interaction computation can only be performed between two bodies, when the origin of one body's coordinate system is outside the circle that circumscribes the other body. This restriction is not constrictive, because the theory presented herein does not include evanescent waves, and so one should only use it at very close separation distances with caution.

In open water, linear theory states that waves are propagating waves with a exponential depth dependence, but near the body, to meet the body boundary condition, evanescent modes fit the propagating wave to the body's shape. Since evanescent waves are neglected in the interaction theory herein, this will naturally lead to errors when bodies are spaced very closely together. One can see these errors in figures 6 and 7 as hydrodynamic quantities and 8 in the wave fields around the bodies. For the 16 cylinder array, the absence of evanescent waves does not effect the computation of motions for an incident wave direction of $\beta = 0$. It does create small errors at $\beta = \frac{\pi}{4}$, but the errors are less than 2% in the body motions and wave field. For the attenuator array, where the body spacing is larger, and more representative of the spacing in a wave farm, the agreement between the motions computed with interaction theory and with the direct BEM computation was excellent. In general, for arrays like wave farms or wind farms, where the spacing is relatively large, the interaction theory can be used with confidence, but for more compact arrays, it should be used with caution and some results should be checked with direct BEM computations.

The interaction theory assumes a constant depth over the domain of the computation. For medium sized arrays, like those shown in figures 9 and 10, constant depth is not unreasonable. However, for the very large array shown in figure 11 it may not be a good assumption. For example, take the atten-

uators to have a beam of $a = 5\,m$, then the area of the wave field computed in that problem would be $0.7\,km \times 3.5\,km$, which may be too large of an area over which to assume a constant depth. Also, herein, only a finite depth theory has been given. Peter and Meylan (2004) extended Kagemoto and Yue (1986)'s theory to infinite depth, but more research is needed to determine how to derived the radiated and scattered wave coefficients following the methodology given here.

Another assumption that may be dubious for such a large array is that the incident wave is a coherent long-crested wave. Using the large array example above, this would be a $3.5\,km$ long crest. The coherent motions and standing waves found throughout the entire array that result from such an incident wave will likely not exist in reality. However, locally over a smaller array subset, there may be such coherent interactions.

The linear wave interaction theory is probably best applied to medium sized arrays, where the bodies are not spaced too closely together, and the flat bottom and long-crested incident wave assumptions are reasonable. Because of the significant speed up afforded by the interaction computation, the method can be employed as a tool for the optimization of the layout of the array by iterative calculations. Examples of such problems would be in the design of a wave farm to maximize power production or of an offshore wind farm to minimize loads or body motions.

7. Conclusion

A novel method has been presented to compute the diffraction transfer matrix and the new force transfer matrix by probing a body with a series of incident plane waves. Inputs to the calculation can be derived from standard numerical or experimental measurements. This computation enables the use of a theory for water wave interactions between multiple bodies developed by Kagemoto and Yue (1986), which leads to improvements in array computation time on the order of 10^3 over direct methods. The method was verified with direct method computation using the BEM solver WAMIT for two geometries, a cylinder and an attenuator type WEC, in a variety of array arrangements and wave conditions, but is general and can be applied to arbitrary geometries and modes of motions. The method presented herein neglects evanescent waves, but their effects are shown to be very small - for the 16 cylinder array, the evanescent waves represented about 4% of the wave field near a given body, and decayed exponentially with distance from

the body. For arrays where the inter-device spacing is of practical interest, such as the wave farm examples, evanescent waves are negligible and the interaction theory matches the BEM computation to differences of less than 0.2% for most of the wave field. Finally, two cases of array computations are considered that could only be computed with interaction theory due to the computational acceleration it affords - a medium sized array in spectral seas and a very large array of 101 WECs.

Acknowledgments

The first author is very grateful for the sponsorship that has enabled this research, which he received through the University of Edinburgh Principal's Career Development and Global Research Scholarships. All authors would like to acknowledge the University of Edinburgh's Institute for Energy Systems for supporting their research in fluid dynamics and wave energy conversion.

Abrmowitz, M., Stegun, I., 1964. Handbook of Mathematical Functions with Formulas, Graphs, and Mathematical Tables. National Bureau of Standards, Washington DC.

Chakrabarti, S., Oct. 2000. Hydrodynamic interaction forces on multi-moduled structures. Ocean Engineering 27 (10), 1037–1063.

Child, B., Venugopal, V., 2010. Optimal configurations of wave energy device arrays. Ocean Engineering 37, 1402–1417.

Cruz, J., 2008. Ocean Wave Energy: Current Status and Future Prespectives (Green Energy and Technology). Springer.

Fenton, J. D., 1978. Wave forces on vertical bodies of revolution. Journal of Engineering Mathematics 85 (2), 241–255.

Garrett, C. J. R., 1971. Wave forces on a circular dock. Journal of Fluid Mechanics 46 (1), 129–139.

Goo, J.-S., Yoshida, K., 1990. A numerical method for huge semisubmersible responses in waves. Transactions of the Society of Naval Architects and Marine Engineers 98, 365–387.

Holthuijsen, L. H., 2007. Waves in Oceanic and Coastal Waters. Cambridge University Press, Cambridge.

Kagemoto, H., Yue, D., 1993. Hydrodynamic interaction analyses of very large floating structures. Marine structures 6, 295–322.

Kagemoto, H., Yue, D. K.-P., 1986. Interactions among multiple three-dimensional bodies in water waves: an exact algebraic method. Journal of Fluid Mechanics 166, 189–209.

Kashiwagi, M., 2000. Hydrodynamic interactions among a great number of columns supporting a very large flexible structure. Journal of fluids and structures 14, 1013–1034.

MacCamy, R. C., Fuchs, R. A., 1954. Wave forces on piles: a diffraction theory. Technical Memorandum No. 69, U. S. Army Corps of Engineers.

Martin, P. A., 2006. Multiple Scattering: Interaction of Time-Harmonic Waves with N Obstacles. Cambridge University Press, Cambridge, UK.

MATLAB R2013a, 2013. The MathWorks, Inc., Natick, MA.

McNatt, J. C., Venugopal, V., Forehand, D., Dec. 2013. The cylindrical wave field of wave energy converters. International Journal of Marine Energy 3-4, e26–e39.

Murai, M., Kagemoto, H., Fujino, M., Dec. 1999. On the hydroelastic responses of a very large floating structure in waves. Journal of Marine Science and Technology 4 (3), 0123–0153.

Newman, J. N., 1977. Marine Hydrodynamics. MIT Press.

Newman, J. N., 1979. Absorption of wave energy by elongated bodies. Applied Ocean Research 1 (4), 189–196.

Newman, J. N., 1997. Wave effects on hinged bodies Part I body motions. Self-published at www.wamit.com/Publications.

Newman, J. N., Lee, C.-H., 2002. Boundary-Element Methods In Offshore Structure Analysis. Journal of Offshore Mechanics and Arctic Engineering 124 (2), 81.

Peter, M. A., Meylan, M. H., Jan. 2004. Infinite-depth interaction theory for arbitrary floating bodies applied to wave forcing of ice floes. Journal of Fluid Mechanics 500 (2004), 145–167.

Peter, M. A., Meylan, M. H., Linton, C. M., Feb. 2006. Water-wave scattering by a periodic array of arbitrary bodies. Journal of Fluid Mechanics 548, 237–256.

Simon, M., 1982. Multiple scattering in arrays of axisymmetric wave-energy devices. Pt. 1: a matrix method using a plane-wave approximation. Journal of Fluid Mechanics 120, 1–25.

WAMIT User Manual, Version 7.0, 2012. WAMIT, Inc.

Wypych, M., Le-Ngoc, L., Alexander, K., Gardner, A., Feb. 2012. On the application of circularcylindrical waves to ocean wave power absorption. Ocean Engineering 40, 69–75.

Yilmaz, O., 1998. Hydrodynamic interactions of waves with group of truncated vertical cylinders. Journal of Waterway, Port, Coastal, and Ocean Engineering 124 (5), 272–279.